

Rectangular waveguide enabling technology using holey surfaces and wire media metamaterials

Stergios Papantonis ^{a,b,*}, Nick M. Ridler ^c, Stepan Lucyszyn ^{a,b}

^a Optical and Semiconductor Devices Group, Department of Electrical and Electronic Engineering, Imperial College London, Exhibition Road, London SW7 2AZ, United Kingdom

^b Centre for Terahertz Science and Engineering, Imperial College London, Exhibition Road, London SW7 2AZ, United Kingdom

^c Time, Quantum and Electromagnetics Division, National Physical Laboratory, Hampton Road, Teddington, Middlesex TW11 0LW, United Kingdom



ARTICLE INFO

Article history:

Received 11 September 2013

Received in revised form 6 January 2014

Accepted 6 January 2014

Available online 20 January 2014

Keywords:

Metamaterials

Wire medium

Pin block

Holey metasurface

Tunable

Reconfigurable

Rectangular waveguide

Filter

Enabling technology

ABSTRACT

A new enabling technology for implementing tunable rectangular waveguide components and circuits is reported for the first time with the use of 2D and 3D metamaterials; a holey metal surface and wire media, respectively. Traditional solid metal irises are replaced by a wire medium metamaterial. These media are well known and used to emulate plasma behavior and, therefore, can be used to replace solid metal. As proof of concepts, results for tunable rectangular waveguide filters are presented with the use of pin block inductive irises and capacitive posts. Furthermore, by adapting the traditional metal-pipe rectangular waveguide for tunability, regions of the solid metal walls are replaced by holey metasurfaces that enable adjustments in the position and spacing of the pin blocks. Prototype tunable structures were measured for verification and good agreement is achieved between full-wave simulations and measurements. The results clearly demonstrate the potential for this tunable/reconfigurable rectangular waveguide enabling technology. Potentially new applications for this permeable enabling technology include lightweight and forced-air/cryogenically cooled subsystems, gas/vapor/humidity/pressure/light sensors, optoelectronic and even real-time tunable/reconfigurable components, circuits and subsystems.

© 2014 Elsevier B.V. All rights reserved.

1. Introduction

Rectangular waveguide technologies have been advancing for many decades and find many applications. Traditional metal-pipe rectangular waveguides (MPRWGs) have been used for extremely low loss applications (e.g., low power radio astronomy to high power radar). Other non-extreme power applications have been implemented with substrate integrated waveguides (SIWs); from the original monolithic metal-pipe [1,2] to the low-cost PCB post-wall (or picket fence) [3] to the next generation of light-pattern-defined “virtual” plasma sidewall REconfigurable Terahertz INtegrated Architecture (RETINA) concept [4,5] for real-time tunable/reconfigurable applications.

The diverse range of MPRWG components, circuits and subsystems make them essential for many microwave and millimeter-wave applications. However, tuning components/circuits and

reconfiguring circuit/subsystem architectures with conventional MPRWG-based technologies can be difficult and/or expensive. To address this issue, tunable metamaterials can be employed [6]. Indeed, the last few decades has seen intensive research in the area of metamaterials with structures having unusual electromagnetic properties. One such material is the so-called wire (or rodded) medium, which has been known to emulate plasma behavior for over half a century [7]. However, it was only recently that a complete physical insight, describing its behavior, was given [8–10]. The wire medium can replace some of the solid metal parts of rectangular waveguide structures with the use of pin blocks. This alone is not enough to make tunable devices, as the issue of adjusting the geometric characteristics remains. For this reason, one further modification is required. Regions of the solid waveguide walls can be replaced by holey metasurfaces, patterned with deeply subwavelength holes [11,12]. The new wall regions provide access to the interior of the waveguide while maintaining its wave-guiding characteristics.

For example, short-circuit tuning stubs can be easily realized by replacing the movable solid metallic end wall with a pin block that can be placed through the holey surface in various positions, as illustrated in Fig. 1(a). As a result, variable delay lines are straightforward to implement, as illustrated in Fig. 1(b), by adjusting the

* Corresponding author at: Optical and Semiconductor Devices Group, Department of Electrical and Electronic Engineering, Imperial College London, Exhibition Road, London SW7 2AZ, United Kingdom.

E-mail addresses: s.papantonis@imperial.ac.uk (S. Papantonis), nick.ridler@npl.co.uk (N.M. Ridler), s.lucyszyn@imperial.ac.uk (S. Lucyszyn).

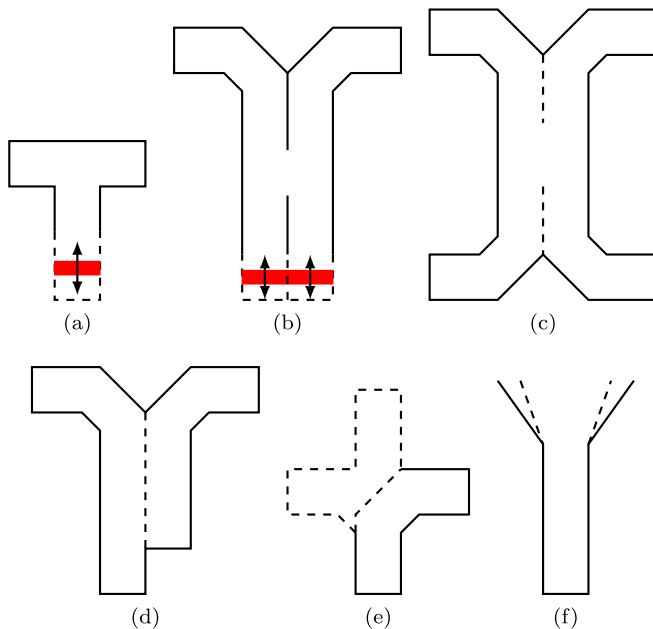


Fig. 1. Concept illustrations of tunable/reconfigurable waveguide components. (a) Short-circuit tuning stub, (b) variable delay line, (c) programmable directional coupler, (d) programmable power splitter, (e) SP3T switch and (f) adjustable H-plane horn antenna. The red sections in (a) and (b) represent moveable pin block. The dashed lines in (c)–(f) represent possible post-wall pin configurations. (For interpretation of the references to color in this legend, the reader is referred to the web version of the article.)

relative position of such tuning stubs and, thus, controlling the effective propagation path length of the guided wave. Similarly, programmable directional couplers with adjustable coupling aperture and tuning posts can be formed, as illustrated in Fig. 1(c), resulting in a change in the coupling coefficient. This concept can also be applied to power splitters, where power ratio can be changed by adjusting their external and internal geometric characteristics, as illustrated in Fig. 1(d). For reconfigurable applications N -throw switches can be realized, e.g., the single-pole three-throw (SP3T) switch shown in Fig. 1(e), where the position of the pins determines the output. Finally, as shown in Fig. 1(f), an adjustable H-plane horn antenna can be realized, where the gain/half-power beamwidth and beam pointing angle of the main lobe can be controlled.

Of course, single- and double-ridged rectangular waveguides can also be implemented, by partially penetrating pins within the waveguide (in the case of double-ridged waveguides both top and bottom walls need to be replaced by the holey metasurface); the penetration depth offers the flexibility of being able to adjust the capacitive loading and hence the guiding properties of the waveguide.

Among the most widely used rectangular waveguide circuits are filters, which can be implemented in a variety of ways; for example, employing inductive and/or capacitive irises, septa or posts [13–16]. For the purposes of demonstrating tunable waveguide circuits using holey surfaces and pin block metamaterials, filters employing inductive irises will be reported, although capacitive irises, septa and posts could also have been used.

2. Filter design

Fig. 2 shows illustrations of a 2-pole tunable inductive iris filter. A metal sheet patterned with an array of holes (arranged in a triangular lattice) to create the metasurface is used to replace small sections of one or more of the traditional MPRWG walls. In addition,

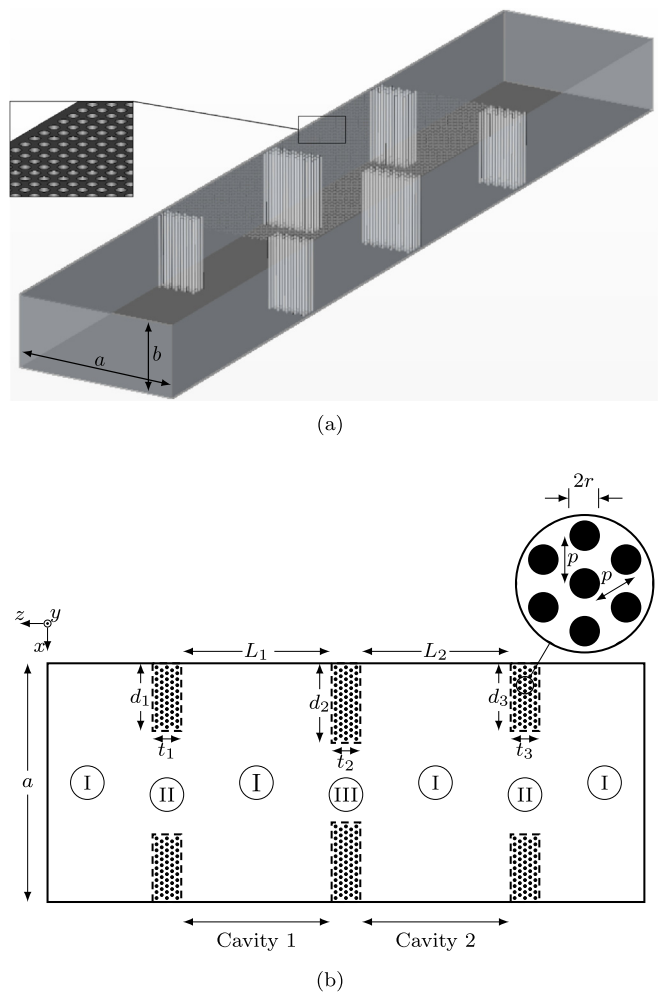


Fig. 2. Proposed filter geometry: (a) isometric view and (b) plan view.

the traditional solid internal field-perturbing metallic elements have been replaced by pin blocks. The result is the implementation of a band pass filter having tunable characteristics from the (re-)positioning of individual pins. The holey metasurface provides the required good electrical characteristics (i.e., sufficiently high conductivity) while enabling to reconfigure the structure mechanically (e.g., by inserting/removing pins through the holes).

Metallic cylindrical pin arrays penetrate the waveguide, via the holes of the metasurface, to create pin block regions that behave as solid metal blocks from a traditional inductive iris, as illustrated in Fig. 2. The physical length of the pins is equal to the external height of the waveguide, with their radius ideally matching that of the holes from the metasurface. The holes have deeply sub-wavelength dimensions, with respect to the guide wavelength (i.e., $r \ll \lambda_g$, where r and λ_g are the radius of the holes and the guide wavelength, respectively) and are arranged in a triangular lattice to minimize the spacing between adjacent pins; maximizing the pin block density and resolution of the individual pin positions. The former is important in order for the pin blocks to better mimic the low loss behavior of the solid blocks; while the latter enables finer tuning resolution.

Due to the perforated periodic pattern of the metasurface, the size and position of the inductive irises can be altered by changing the density and individual positions of pins and, therefore, the pass band can be easily tuned.

For simplicity, the waveguide is operating at the fundamental TE_{10} mode (only E_y , H_x , and H_z are non-zero), so that higher order

Table 1

Spatial dimensions (in mm) of the proposed filter corresponding to triangular lattice hole/pin positions.

f_0	a	b	p	r	$L_1 = L_2$	$d_1 = d_3$	d_2	$t_1 = t_3$	t_2
8.4	23	10	0.75	0.25	24.5	5.82	7.79	2.75	3.5
9.2	23	10	0.75	0.25	19.5	5.82	7.79	3.5	3.5
10.6	23	10	0.75	0.25	14.5	5.82	7.12	3.125	3.5

modes are cut off. Thus, the pins have to be placed vertically (parallel to the electric field) in order for E_y to induce currents along the pins and hence strongly interact with them. It is well known that wave-guiding structures containing discontinuities can be studied analytically using mode-matching techniques. If this technique is applied for the design shown in Fig. 2, where the waveguide is partitioned into several sections, the fields in each section are expanded in normal waveguide modes and the continuity of the fields is enforced at the interfaces. A thorough analysis is beyond the scope of this work and can be found in many standard textbooks (e.g., [17,18]).

2.1. Band pass filter

A 2-pole X-band tunable band pass filter will first be simulated with the use of a rectangular waveguide having approximate internal width a and height b spatial dimensions of $a \times b = 23 \text{ mm} \times 10 \text{ mm}$ (i.e., similar to a standard WR-90 waveguide), with the whole of the top wall (as an extreme case) replaced by the holey metasurface. To create a 2-pole filter, two cavity regions require six pin blocks inside the rectangular waveguide. For this particular filter design, symmetry exists in the $x-z$ plane at $x = a/2$ and also in the $x-y$ plane at the center of the filter; therefore, the physical length of each cavity $L_1 = L_2 = L$ and the first and third irises have the same effective spatial dimensions of depth ($d_1 = d_3$) and thickness dimensions ($t_1 = t_3$). The nominal physical dimensions of the designed structures are given in Table 1.

This metamaterial filter has the important advantage in that it can be easily tuned, where the pass band can be translated across the entire X-band. The resonant frequency of the cavities (which defines the center frequency of the pass band f_0) is mainly affected by separation distance L . However, in order to fine tune the performance of the filter, other parameters can be adjusted, as will be discussed later. As an example, the results of full-wave numerical simulations using CST microwave studio (MWS) are shown in Fig. 3, for a filter having holey surfaces and pin block metamaterials defined by the physical dimensions given in Table 1. Moreover, but not shown here, the bandwidth of the pass band can just as easily be controlled by varying the depths d_1-d_3 to achieve the required coupling coefficient, by tuning levels of shunt inductive coupling.

A lumped-element equivalent circuit model for the 2-pole filter demonstrator is shown in Fig. 4. It consists of two directly coupled series $L_R C_R$ resonators, which describe the identical cavity resonators in the waveguide filter, and three inductive coupling elements that correspond to the inductive irises (i.e., L_{11} and L_{12}) formed by the pin blocks. Finally, $Z_{TE_{10}} = \omega\mu/k_z$ is the transverse wave impedance for the dominant TE_{10} mode, with μ being the magnetic permeability of the waveguide filler (i.e., air in this case, with $\mu = \mu_0$), $k_z = \sqrt{\beta^2 - (\pi/a)^2}$ is the wavevector for the TE_{10} mode along the direction of propagation and the phase constant in free space $\beta = \omega/c$, with ω and c being the angular frequency and the speed of light in free space, respectively.

Numerical simulation results clearly show that, within the pass band, both cavities are excited at resonance and most of the power propagates along and through the waveguide. Moreover, the

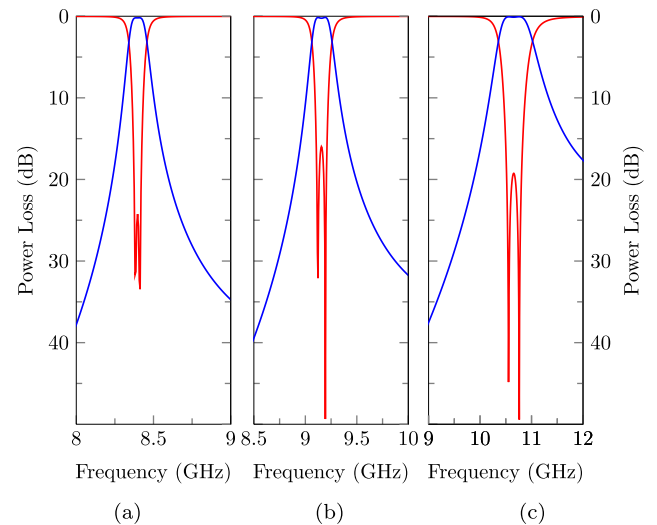


Fig. 3. Numerical simulation results of transmission (blue curves) and reflection (red curves) power loss characteristics for a tunable filter using the parameters given in Table 1, having its center frequency tuned for: (a) 8.4 GHz; (b) 9.2 GHz; and (c) 10.6 GHz. (For interpretation of the references to color in this legend, the reader is referred to the web version of the article.)

physical spacing L is approximately half the guided wavelength, as seen in Fig. 5. Conversely, outside the pass band, the cavities are excited but the evanescent electric field decays exponentially through the cavities; the result is that the output power is just a small fraction of the input power.

To further investigate the performance of the holey surfaces and pin block metamaterials filter, and understand the effect of the various design parameters on its operation, parametric analysis has been undertaken, with some results shown in Fig. 6. Specifically, Fig. 6(a)–(d) was obtained by adding/removing a row of pins in the dimension of interest. It can be seen that resonance is sensitive to changes in d_1 , d_2 and t_2 ; even small variations in these parameters may completely distinguish the resonance. However, t_1 can be used to fine tune the pass band characteristics. As expected, different scenarios can yield similar results. For example, Fig. 6(e) and (f) shows that appropriate combinations for the values of d_1 and d_2 can shift the pass band, similar to adjusting the length L (i.e., increasing d_1 and d_2 increases the shunt inductance, which effectively reduces the electrical length of the cavities, similar to reducing L). Thus, there are many degrees of freedom that can be used to tune the filter.

2.2. Band stop filter

Another example of a simple tunable device is that of a band stop filter, realized by employing capacitive posts [15]. Even a single pin

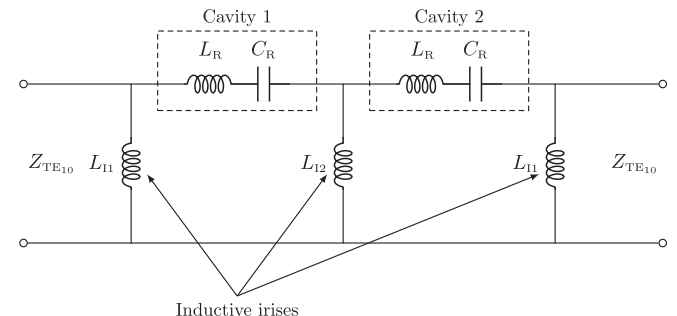
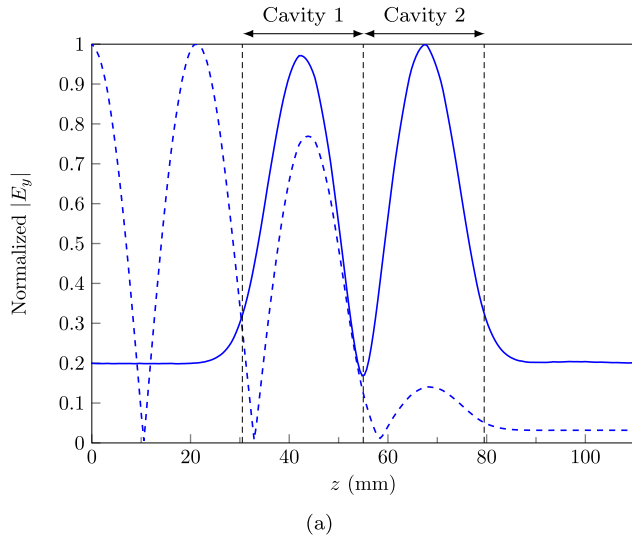
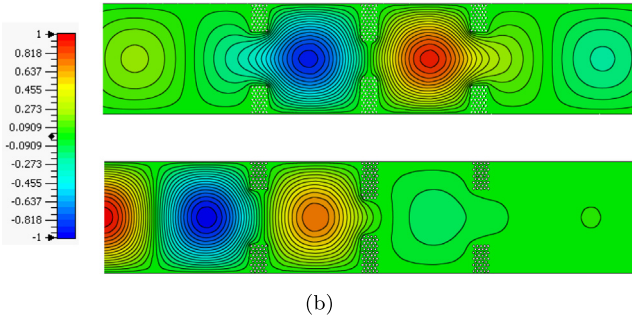


Fig. 4. Ideal lumped-element equivalent circuit model for the 2-pole filter demonstrator.



(a)



(b)

Fig. 5. (a) Numerical simulation results of normalized magnitude of E_y in the pass band at 9.2 GHz (solid curves) and outside the pass band at 9.5 GHz (dashed curves) and (b) corresponding contour plots of E_y in the pass band (top) and outside the pass band (bottom), respectively.

that partially penetrates the inside of the waveguide can be used to implement the band stop characteristic [15]. The center frequency can be tuned by adjusting the penetration ratio h/b of the pin, where h is the internal penetration length of the pin (the smaller the ratio, the higher the tuned frequency), as can be seen in Fig. 7.

3. Manufactured proof-of-concept demonstrators

3.1. Band pass filter

A prototype of the 2-pole tunable filter, described in Section 2, has been fabricated. A single 0.5 mm thick perforated aluminum sheet having periodically arranged holes (with diameter $2r=0.5$ mm, in triangular lattice and with 1 mm periodicity) has been wrapped around a standard WR-90 rectangular waveguide filler, as shown in Fig. 8(a). The longitudinal gap along the length of the waveguide was sealed with a narrow strip of conductive aluminum tape. The joint was placed in the center of the broad wall of the waveguide (where the electric field is at a maximum for the fundamental mode), in order to ensure a good electrical connection at the critical locations where the electric field is zero. Next, 0.5 mm diameter stainless steel pins are inserted through the rectangular waveguide, in order to form the pin blocks for the inductive irises, as shown in Fig. 8(b) and (c); after tuning, the pins are secured in place with conductive epoxy glue.

Measurements were undertaken at the UK's National Physical Laboratory, using a vector network analyzer (VNA) having a pair of WR-90 waveguide test ports and associated traceable calibration standards, for accurate S-parameter measurements across

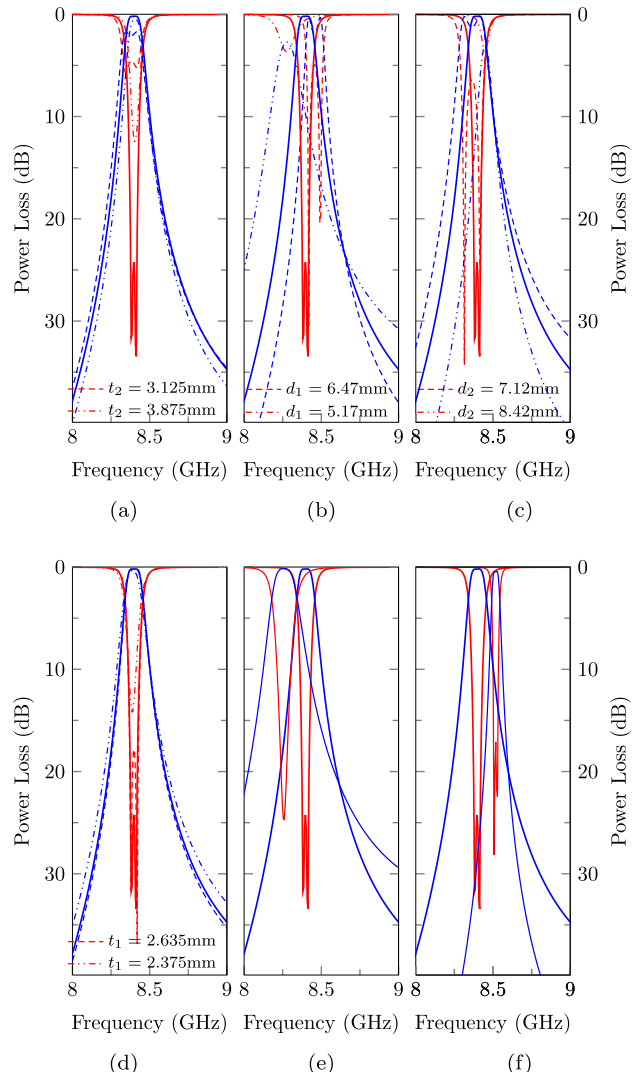


Fig. 6. Numerical simulation results of transmission (blue curves) and reflection (red curves) power loss characteristics for various parametric studies. Thick lines correspond to the values shown in Table 1: (e) $d_1 = 5.17$ mm, $d_2 = 7.12$ mm and (f) $d_1 = 6.47$ mm, $d_2 = 8.42$ mm. (For interpretation of the references to color in this legend, the reader is referred to the web version of the article.)

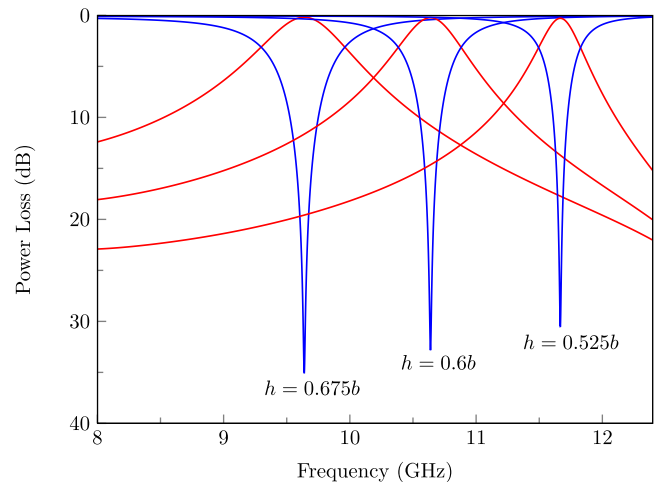


Fig. 7. Numerical simulation results of transmission (blue curves) and reflection (red curves) power loss characteristics for various penetration ratio values. (For interpretation of the references to color in this legend, the reader is referred to the web version of the article.)

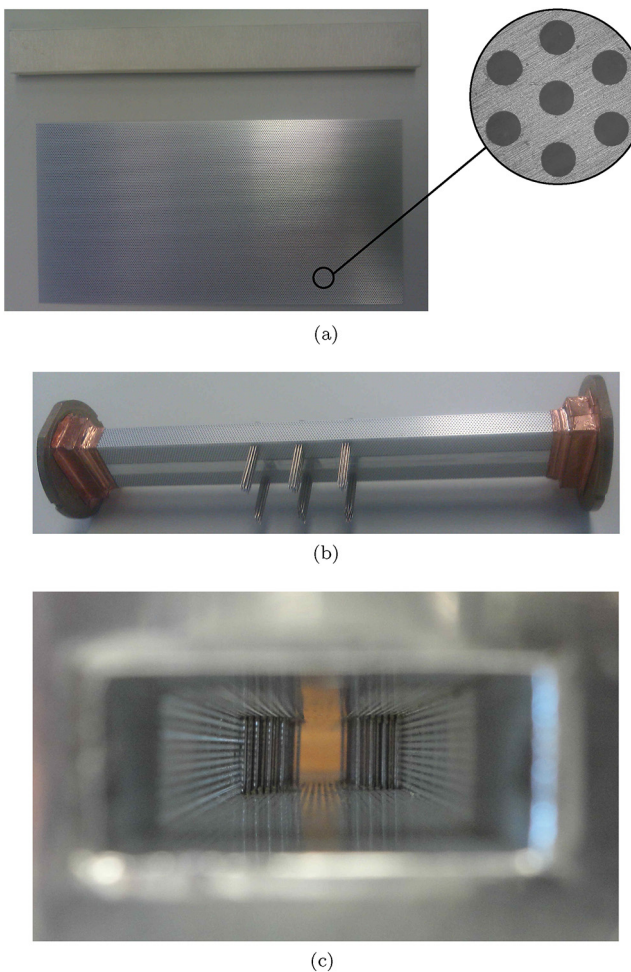


Fig. 8. (a) Above: modified WR-90 dielectric filler (used as a temporary former) and below: flat $20 \times 10 \text{ cm}^2$ perforated aluminum sheet (before assembly); (b) underside of the prototype filter (where the aluminum tape, protruding pins and standard WR-90 flanges can be seen); and (c) transverse view through the filter (showing the pin blocks and metasurfaces on all four walls running along the entire length of the 20 cm long rectangular waveguide).

the 8.2–12.4 GHz frequency range. Thru-Reflect (short)-Line (TRL) calibration [19] establishes the measurement reference planes at the waveguide test ports. The calibration was performed using an external calibration algorithm, employing a seven-term error-correction routine [20]. The complete measurement set-up (i.e., VNA, primary standards and calibration algorithm) is referred to as the NPL primary impedance microwave measurement system (PIMMS) [21,22], and represents the UK's primary national standard system for S-parameter measurements. PIMMS also determines the uncertainty in the S-parameter measurements. This is achieved following internationally agreed guidelines [23], with minor modifications to accommodate the complex-valued (i.e., vector) nature of the S-parameter measurands [24]. For measurements in WR-90 waveguide, uncertainties of the linear magnitude of transmission coefficients typically range from 0.0003 to 0.0005 for a nominal transmission of 0.1 (i.e., 20 dB) in this waveguide band. Similarly, uncertainties for measurements of the linear magnitude of reflection coefficients typically range from 0.001 to 0.003 for low reflecting devices.

As can be seen in Fig. 9, a 2nd-order Chebyshev filter response, having two return loss zeros, is obtain when $d_1 = d_3 = 6.4 \text{ mm}$, $d_2 = 7.3 \text{ mm}$, $t_1 = t_3 = 3 \text{ mm}$ and $t_2 = 4.5 \text{ mm}$; whereas Fig. 10 shows the filter tuned to have a Butterworth type response. This can be achieved by changing the inductive coupling elements (i.e.,

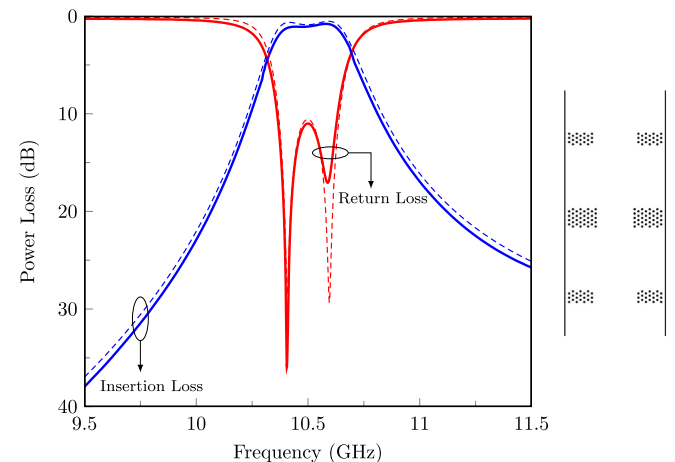


Fig. 9. Left: Chebyshev filter full-wave CST MWS simulated (dotted curves) and measured (solid curves) responses; right: individual pin arrangement with $L=L_1=L_2=14.5 \text{ mm}$.

changing the number and location of pins). Here, for example, $d_1 = d_2 = 6.5 \text{ mm}$, $d_3 = 4.6 \text{ mm}$ and $t_1 = t_2 = t_3 = 3 \text{ mm}$. The agreement between simulated and measured results is excellent in both cases, with only small discrepancies being attributed to manufacturing tolerances on the specified dimensions. The 1.4 % shift in frequency can be easily corrected by a small increase in $L=L_1=L_2=15 \text{ mm}$.

It is interesting to note that the in-band insertion losses for both filters are approximately 0.5 dB in X-band, which includes the use of non-ideal metals (i.e., lossy aluminium for the holey metasurfaces and stainless steel for the pin blocks) and the additional contributions from the two superfluous 13.1 cm long aluminium holey metasurface feed lines; clearly indicating that this technology is inherently low loss. Obviously, the insertion loss performance for these filters can be improved by using copper (instead of both aluminium and stainless steel) and removing the long feed lines.

3.2. Band stop filter

Next, a prototype of a simple single-pole band stop filter is fabricated by inserting a single pin partially inside an unperturbed rectangular waveguide, as described previously. The pin is located off center [15]. The response of this device is shown in Fig. 11, where the agreement between simulated and measured results is again

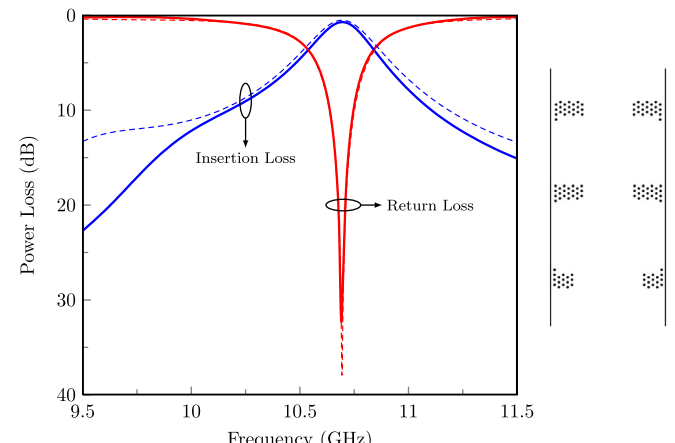


Fig. 10. Left: Butterworth filter full-wave CST MWS simulated (dotted curves) and measured (solid curves) responses; right: individual pin arrangement with $L=L_1=L_2=14.8 \text{ mm}$.

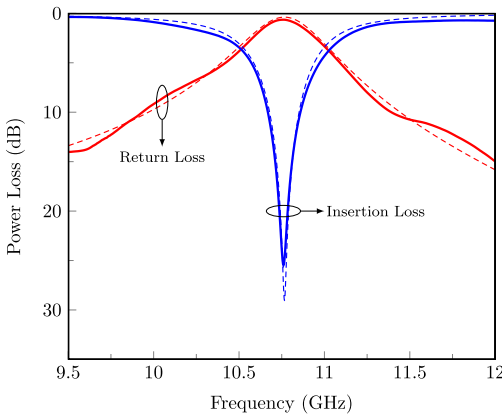


Fig. 11. Left: single capacitive post-pin band stop filter full-wave CST MWS simulated (dotted curves) and measured (solid curves) responses; right: single pin having a penetration ratio $h/b = 0.59$ and 3.7 mm offset from center.

excellent. The peak value of in-band return loss is approximately 0.6 dB.

3.3. Single resonator

Taking advantage of the structure's flexible arrangement for tunability, a single cavity resonator has been created by placing two double-rows of pins across the transverse width of the waveguide, separated by a distance $L = 15.3$ mm. Thus, the textbook value for the lossless resonant frequency of the dominant fundamental TE₁₀₁ mode can be approximated by the well-known expression $f_{101} = [c\sqrt{(\pi/a)^2 + (\pi/L)^2}]/2\pi$. In order to increase the coupling efficiency, the middle pin of each row is removed. Further pins can be removed, in order to obtain stronger coupling, but at the expense of decreasing the loaded quality factor. On the other hand, the loaded quality factor is increased if none of the pins are removed (i.e., weaker coupling). The simulated and measured responses for this simple resonant structure are shown in Fig. 12, where any discrepancy between simulated and measured values is due to the poor repeatability of our simple prototype.

The loaded quality factor $Q_L(f_0)$ can be obtained from the transmission coefficient, either using the -3 dB bandwidth (i.e., $Q_L(f_0) = \Delta f/f_0$, where Δf and f_0 are the -3 dB bandwidth and the

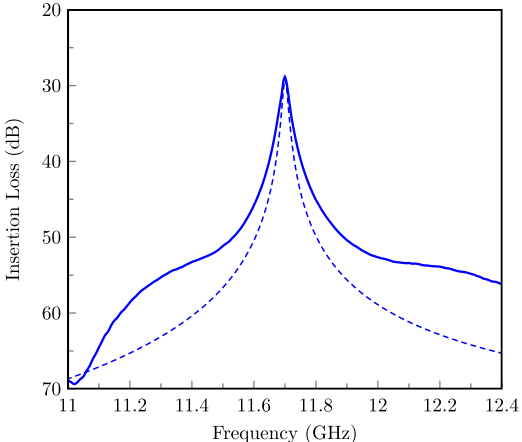


Fig. 12. Left: cavity resonator full wave CST MWS simulated (dotted curve) and measured (solid curve) insertion loss responses; right: pin arrangement with internal spatial dimensions of $a \times b \times L = 23 \times 10 \times 15.3$ mm³.

Table 2
Loaded and unloaded quality factors for the cavity shown in Fig. 12.

	Simulated	Measured
Unloaded $Q_u(f_0)$	698	419
Loaded $Q_L(f_0)$	677	402

resonant frequency, respectively) or from the insertion phase frequency response by

$$Q_L(f_0) = \frac{f_0}{2} \left. \frac{\partial \angle S_{21}(f)}{\partial f} \right|_{f=f_0} \quad (1)$$

Both definitions are equivalent for large Q_L and give the same result (within a small numerical margin of error). The unloaded quality factor $Q_u(f_0)$ can be calculated by taking into account the loading of the cavity from

$$Q_u(f_0) = \frac{Q_L(f_0)}{1 - |S_{21}(f_0)|} \quad (2)$$

The results for both $Q_L(f_0)$ and $Q_u(f_0)$ are given in Table 2. As can be seen, there is a difference between simulated and measured results for such high Q-factor resonators. This is mainly because of pin misalignment with our simple prototypes (since there are only two rows of pins). However, when the unloaded quality factor is compared with classical waveguide resonators (i.e., fixed structures having no tuning ability), there is a reduction in performance. This is because tunability comes at the cost of increased losses both via radiation through the holes and power leakage through the rows of pins (i.e., power that does not contribute to the resonance). Fortunately, these losses can be dramatically reduced by: (1) decreasing the size of the holes; (2) having only a small section of the waveguide patterned with such holes; and (3) increasing the pin density.

4. Discussion

The holey metasurface can be described as an effective medium, using homogenization concepts, having an effective conductivity σ_{eff} dictated by a filling factor; being naturally lower than the bulk dc conductivity σ_0 of conventional solid walls (i.e., $\sigma_{eff} < \sigma_0$). Although such a structure can expect to have slightly higher losses, due to the small amount of radiation through the holes,

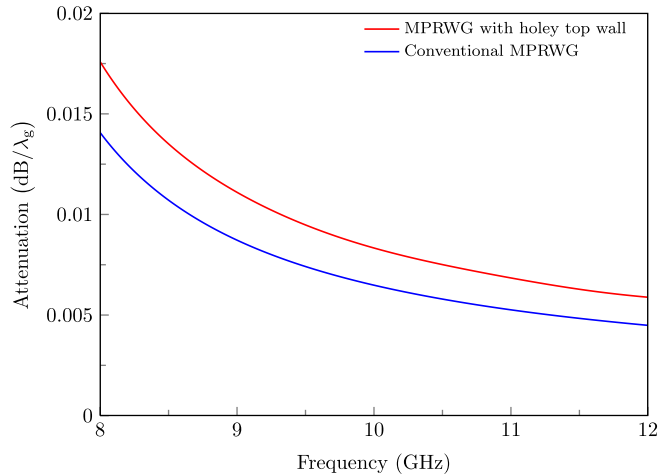


Fig. 13. Numerical simulation results of attenuation per guided wavelength in X-band for a conventional aluminum WR-90 rectangular waveguide and one whose top wall is replaced by the proposed holey metasurface having dimensions given in Table 1.

when compared with a conventional MPRWG, the losses can be dramatically reduced.

Fig. 13 shows the attenuation of the proposed waveguide having a metasurface on the whole of its top wall (without any pins) and a conventional MPRWG. In practice, the losses can be reduced almost back to the levels of the conventional MPRWG by covering the remaining holes with a conductive adhesive metal foil after tuning with simple physical or automated actuation mechanisms.

5. Conclusion

A new and generic enabling technology for realizing rectangular waveguide-based tunable components and circuits, which combines 2D and 3D metamaterials (holey metasurfaces and pin blocks, respectively), has been demonstrated for the first time. Two classical filter implementations have been demonstrated. The first employs tunable inductive iris to retune from the Chebyshev to Butterworth approximations for a 2-pole band pass filter; while the second employs a capacitive post to achieve a band stop filter characteristic having a single-pole Butterworth approximation.

The parametric study has shown robustness to the restriction of pin location and manufacturing tolerances. Moreover, with its large degrees of tuning freedom, which lends itself to automation, this technology can achieve high levels of functionality. Moreover, the measured low loss performances of the experimental filters, as well as the high Q-factors for a single resonator, given the non-ideal lossy metals used, clearly demonstrate that this new metamaterials technology can provide a low cost solution for tunable and reconfigurable architectures.

The proposed technology may find many applications that are not just limited to high performance filters that have restrictions on manufacturing tolerances [25,26]. Many types of discontinuity can be easily introduced by inserting pins either fully or partially into the rectangular waveguide and in all three orthogonal planes. For example, tunable ridged waveguides is one possible application. Moreover, the post-wall SIW, with its diverse array of component and circuits, including all the examples illustrated in **Fig. 1**, is a natural application of this technology, as the sidewall vias can be replaced by tunable pin arrays with block actuators.

Finally, potentially new applications for this permeable enabling technology include lightweight and forced-air/cryogenically cooled subsystems, gas/vapor/humidity/pressure/light sensors, optoelectronic and even real-time tunable/reconfigurable components, circuits and subsystems. Here, a resonance or series of resonances can be implemented and the resulting frequency detuning and reduction in quality factors can be detected, giving valuable information on the particular parameter under test.

Acknowledgment

This work was supported in part by the ARFTG Student Fellowship.

References

- [1] S. Lucyszyn, Q.H. Wang, I.D. Robertson, 0.1 THz rectangular waveguide on GaAs semi-insulating substrate, *IEE Electron. Lett.* 31 (9) (1995, April) 721–722.
- [2] S. Lucyszyn, D. Budimir, Q.H. Wang, I.D. Robertson, Design of compact monolithic dielectric-filled metal-pipe rectangular waveguides for millimetre-wave applications, *IEE Proc. Microw. Antennas Propag.* 143 (5) (1996, October) 451–453.
- [3] K. Wu, Integration and interconnect techniques of planar and nonplanar structures for microwave and millimeter-wave circuits – current status and future trend, in: Asia Pacific Microwave Conference, 2001, pp. 411–416.
- [4] S. Lucyszyn, Y. Zhou, Reconfigurable terahertz integrated architecture (RETINA), in: 33rd International Conference on Infrared, Millimeter, and Terahertz Waves (IRMMW-THz 2008), Pasadena, USA, 2008, September.
- [5] Y. Zhou, S. Lucyszyn, Modelling of reconfigurable terahertz integrated architecture (RETINA) SIW structures, *PIER J.* 105 (2010, June) 71–92.
- [6] K. Herbertz, S. Lucyszyn, Electromagnetic bandgap filter with single-cell monolithic microwave integrated circuit-tunable defect, *IET Microw. Antennas Propag.* 4 (8) (2010, August) 1123–1131.
- [7] W. Rotman, Plasma simulation by artificial dielectrics and parallel-plate media, *IRE Trans. Antennas Propag.* 10 (1962) 82–95.
- [8] M.G. Silveirinha, Nonlocal homogenization model for a periodic array of ε -negative rods, *Phys. Rev. E* 73 (2006) 046612.
- [9] M.G. Silveirinha, C.A. Fernandes, Transverse-average field approach for the characterization of thin metamaterial slabs, *Phys. Rev. E* 75 (2007) 036613.
- [10] S.I. Maslovski, M.G. Silveirinha, Nonlocal permittivity from a quasistatic model for a class of wire media, *Phys. Rev. B* 80 (2009) 245101.
- [11] D. Ramaccia, F. Bilotti, A. Toscano, Analytical model of metasurface consisting of a regular array of sub-wavelength circular holes in a metal sheet, *PIER M.J.* 18 (2011) 209–219.
- [12] D. Ramaccia, G. Bellaveglia, R.L. Forti, Inductive tri-band double element FSS for space applications, *PIER C.J.* 18 (2011) 87–101.
- [13] Y. Zhai, Q. Wang, Z. Wang, X.X. Gao, The design of an iris filter at 37.5 GHz, in: Global Symposium on Millimeter Waves, 2008, pp. 348–350.
- [14] S. Li, J. Fu, X. Wu, Analysis of high-power rectangular waveguide filter with capacitive coupling iris for satellite, in: APPEEC, 2009.
- [15] U. Rosenberg, S. Amari, A novel band-reject element for pseudoelliptic band-stop filters, *IEEE Trans. Microw. Theory Tech.* 55 (4) (2007) 742–746.
- [16] R. Gesche, N. Loeschel, Two cylindrical obstacles in a rectangular waveguide-resonances and filter applications, *IEEE Trans. Microw. Theory Tech.* 37 (6) (1989) 962–968.
- [17] R.E. Collin, *Field Theory of Guided Waves*, 2nd ed., IEEE Press, New York, USA, 1991.
- [18] C.A. Balanis, *Advanced Engineering Electromagnetics*, Wiley, New York, USA, 1989.
- [19] G.F. Engen, C.A. Hoer, Thru-Reflect-Line: an improved technique for calibrating the dual six port automatic network analyser, *Trans. Microw. Theory Tech.* 27 (12) (1979, December) 987–993.
- [20] A. Rumiantsev, N.M. Ridler, VNA calibration, *IEEE Microw. Mag.* 9 (3) (2008, June) 86–99.
- [21] N.M. Ridler, A review of existing national measurement standards for RF and microwave impedance parameters in the UK, in: IEE Colloquium Digest, No. 99/008, 1999, February, pp. 6/1–6/6, February.
- [22] N.M. Ridler, News in RF impedance measurement, in: XXVII General Assembly of the International Union of Radio Science (URSI), Maastricht, 2002, August.
- [23] ISO/IEC Guide 98-3:2008, *Uncertainty of Measurement – Part 3: Guide to the Expression of the Uncertainty in Measurement (GUM:1995)*, International Organization for Standardization, Geneva, Switzerland, 2008.
- [24] N.M. Ridler, M.J. Salter, An approach to the treatment of uncertainty in complex S-parameter measurements, *Metrologia* 39 (3) (2002, June) 295–302.
- [25] C. Chrisostomidis, S. Lucyszyn, On the theory of chained-function filters, *IEEE Trans. Microw. Theory Tech.* 53 (10) (2005, October) 3142–3151.
- [26] C. Chrisostomidis, S. Lucyszyn, Seed function combination selection for chained function filters, *IET Microw. Antennas Propag.* 4 (6) (2010, June) 799–807.

Biographies



Stergios Papantonis was born in Hannover, Germany, in 1986. He received the Dipl.-Ing. degree in electrical and computer engineering from the University of Patras, Greece, in 2010. He is currently working toward the Ph.D. degree at Imperial College London, UK. His main research interests are in the areas of metamaterials and electromagnetic wave propagation and terahertz passive components. He was the recipient of the 2012 ARFTG Student Fellowship award.



Nick M. Ridler received the B.Sc. degree from the University of London, UK, in 1981. He has since spent more than 30 years working in both industrial and government scientific research laboratories. He is currently employed by the National Physical Laboratory, UK, where he is a Principal Research Scientist involved in high-frequency precision measurement activities. His current research interests include measurements at millimeter and sub-millimeter wavelengths and high-speed digital signal measurements on printed circuit boards. Mr. Ridler was the President (2011–2013) of ARFTG (the Automatic RF Techniques Group); Past Chair (2010–2012) of the IEEE MTT-11 “Microwave Measurements” Technical Committee; Chair of IEEE Standard Working Group P1785 “Waveguide for Millimeter and Submillimeter Wavelengths”; Vice-chair of IEEE Standard Working Group P287 “Precision Coaxial Connectors at RF, Microwave and Millimeter-wave Frequencies”; Vice-chair of the MTT-S Standards Coordinating Committee; and, Member of the IEEE MTT-4 “Terahertz Technology and Applications” Technical Committee. He is a Chartered Engineer and a Fellow of the Institution of Engineering and Technology (formerly the Institution of Electrical Engineers, UK). In 2013 he was elevated to Fellow of the IEEE (Class of 2014).



Stepan Lucyszyn received his Ph.D. degree in electronic engineering from King's College London (University of London) and D.Sc.(higher doctorate) degree in millimeter-wave and terahertz electronics from Imperial College London in 1992 and 2010, respectively. He is currently a Reader (Associate Professor) in Millimeter-wave Electronics and Director of the Centre for Terahertz Science and Engineering, at Imperial College London. After working in industry, as a satellite systems engineer for maritime and military communications, he spent the first 12 years researching microwave and millimeter-wave RFIC/MMICs, followed by RF MEMS technologies. For over 17 years, Dr Lucyszyn has been working on millimeter-wave electronics and, since 2004, investigating the behavior of materials, passive structures and ubiquitous applications at THz frequencies. For the past 16 years he

has been teaching 'MMIC Measurement Techniques' at the UK's National Physical Laboratory. He has (co-)authored approximately 150 papers and 11 book chapters in applied physics and electronic engineering, and delivered many invited presentations at international conferences. From 2005 to 2009 he served as an associate editor for the *IEEE/ASME Journal of Microelectromechanical Systems*. In 2011, Dr Lucyszyn was the Chairman of the 41st European Microwave Conference, held in Manchester (UK). In 2005, he was elected as a Fellow of the Institution of Electrical Engineers (UK) and Fellow of the Institute of Physics (UK), and in 2008 was invited as a Fellow of the Electromagnetics Academy (USA). In 2009 he was appointed an IEEE Distinguished Microwave Lecturer (DML) for 2010–2012 and Emeritus DML for 2013. In 2013 he was made a European Microwave Lecturer (EML) for the European Microwave Association and elevated to Fellow of the IEEE (Class of 2014).